

**Quantitative Trace Level Voltammetry in Biological Solution Mimics:
Comparison of Single-Walled Carbon Nanotube Network
Electrodes and Screen-Printed Carbon Electrodes**

Sharel P. E,^{‡,†} Thomas S. Miller,^{‡,§} Lingcong Meng,^{‡,¶} Patrick R. Unwin^{*‡} and Julie
V. Macpherson^{*‡}

[†]School of Health & Life Sciences, Teesside University, Middlesbrough, TS1 3BX, UK

[‡]Department of Chemistry, University of Warwick, Coventry, CV4 7AL, UK

[§]Electrochemical Innovation Lab, Department of Chemical Engineering, University College
London, Torrington Place, London WC1E 7JE, UK

[¶]School of Chemistry, University of Southampton, Southampton SO17 1BJ, UK

E-mail: j.macpherson@warwick.ac.uk, p.r.unwin@warwick.ac.uk; Fax: (+44) 02476 524112

Abstract

Single walled carbon nanotube (SWNT) network electrodes, in which a planar arrangement of SWNTs on an inert surface serves as a working electrode for voltammetry or amperometry, offer considerable attributes for electroanalysis. Here, the effect of SWNT network density on trace voltammetric analysis in biological solution mimics is investigated. In particular, we focus on polymeric solutions containing either polyethylene glycol (PEG) or albumin, used in aqueous solutions to simulate cellular-biology environments. Comparison is made between SWNT network electrodes, grown by catalyzed chemical vapour deposition (CVD) at three different surface coverages (density), 5, ~ 20 and $\sim 30 \mu\text{m}_{\text{SWNT}} \mu\text{m}^{-2}$, and commercial screen-printed carbon electrodes (SPCEs). The one-electron oxidation of ferrocenecarboxylic acid (FcCOOH) is employed as an example redox system to test the response of the electrodes. In 8% PEG 2K, SWNT electrodes outperform SPCEs irrespective of the coverage. For cyclic voltammetry, the lowest detectable concentration decreases as SWNT network density increases. However, when employing differential pulse voltammetry, all three networks show a similar limit of detection, 1 nM FcCOOH, three orders of magnitude lower than achievable for SPCEs. This is attributed to the low capacitance of the SWNTs and absence of amorphous carbon structures which can contribute a pseudo-capacitive response. Repeat cycling in both PEG and albumin solutions shows the higher density SWNT network electrodes ($\geq 20 \mu\text{m}_{\text{SWNT}} \mu\text{m}^{-2}$) to be far less susceptible to electrode fouling, than the low density network, as inferred from the electrochemical response for FcCOOH electro-oxidation. Toward practical devices, a three-electrode chip, similar in design to that used in SPCEs, with patterned high density SWNT networks functioning as the working and counter electrodes, is demonstrated to have impressive detection sensitivity (nM) in PEG solutions. The simplicity and practicality of the design widens the potential applications of these ultra-sensitive diagnostic tools based on planar SWNTs grown by CVD.

Keywords: single walled carbon nanotubes, nanomolar detection, differential pulse voltammetry, albumin, polyethylene glycol, screen printed carbon electrode, electroanalysis

Introduction

Carbon-based electrochemical (EC) sensors have become the subject of intense investigation for applications in many areas including biotechnology [1] and clinical applications [2, 3]. In particular, screen-printed carbon electrodes (SPCEs) are popular [4-6] due to their reproducible manufacture in high volumes leading to low cost and disposability [7]. However, a limitation of SPCEs is that the commercial ink formulations, containing carbon particles, such as graphite, carbon black and activated carbon, and non-conducting binders such as polyvinylidene fluoride and polycarbonate, are usually unknown to the researcher (customer). Moreover, the various ink components can affect the EC properties in different ways [8] and the background currents of such electrodes can be significant, containing both non-faradaic and pseudo-capacitive contributions. Finally, the highly heterogeneous structure [9] can vary from one electrode device to another [10].

Carbon nanomaterials are providing improvements in the stability, sensitivity, and selectivity of electrochemical detectors [11, 12]. Among carbon nanomaterials, single-walled carbon nanotubes (SWNTs) have attracted particular interest in EC analysis due to their promising physical [13] and chemical [14] properties, including chemical stability [15], biocompatibility [13], high sensitivity [16] and low background currents [13]. However, the method of growth and preparation can also impact the resulting EC response. SWNTs grown by non-chemical vapour deposition (CVD) methods, e.g. electric arc discharge, typically contain appreciable levels of impurity catalytic nanoparticles and amorphous carbon that will contribute to the EC response, unless appropriately cleaned before use [13, 17]. SWNT electrodes prepared by dispersing the nanotubes onto a conducting electrode substrate by spin-coating, drop casting [18, 19] or printing [20], can show interference in the EC response from the support material [21]. These methods can also result in high and uneven coverages of the SWNTs, and large

background currents [22], [23]. In contrast, the direct growth of SWNTs on insulating substrates using catalytic CVD [24] provides electrodes with controllable surface coverage, spanning 1D, 2D and 3D arrangements [13]. Moreover, the resulting SWNTs have a low defect density [25], low amorphous carbon content and are relatively free of catalytic nanoparticles (NPs) [26], such that post-growth cleaning or treatments are not required.

The ability to control the growth density and SWNT arrangement is important as the non-faradaic, or background, current is an important issue for the practical sensitivity of amperometric/voltammetric sensors. The background current typically scales with electrode area [27]. A further issue for any EC device is possible electrode fouling during use, resulting in changes to the EC response, detection limit and the lifetime of an EC sensor. Previous work from our group showed that increasing the surface coverage of SWNTs on a silicon oxide substrate helped to mitigate electrode fouling effects due to the higher density of active electrode material and/or the lower mass transport per SWNT length during EC operation [26-29]. Thus, where fouling could be a problem, but a low-level of detection sensitivity is required, careful tailoring of SWNT coverage in an electrochemical (voltammetric) sensor is extremely important.

Ferrocene and its derivatives [30, 31] and other electroactive moieties such as ruthenium [32], and osmium complexes [33] are often used as EC redox-labels, in e.g. the detection of nucleic acids [34, 35]. This is due to the well-understood electrochemistry (fast electron transfer leading to diffusion-limited processes at moderate potentials), high stability and synthetic simplicity [35]. We have thus selected ferrocene carboxylic (FcCOOH) acid as the redox probe for the studies herein.

To examine the effect of potential fouling agents, we have considered polyethylene glycol (PEG) and albumin. PEG is a highly water-soluble and nontoxic polymer [36]. It is often used in biosensor applications to simulate the cellular environment, due to its ability to mimic the excluded volume effect of proteins and act as a crowding agent [37-39]. However, the adsorption of PEG on carbon nanotubes can cause surface passivation which impacts EC detection deleteriously [40]. EC detection signals may also be compromised due to the diminished diffusion coefficients of soluble analytes in high viscosity concentrated PEG solutions. Albumin is the most abundant protein found in blood plasma and can also be used as a crowding agent [41]. Albumin is regarded as a good model to investigate the influence of bio-fouling on the performance of EC sensors [29].

In this paper, we examine the effect of SWNT surface coverage on the EC detection limit of FcCOOH in the presence of first PEG and then albumin. The SWNTs are grown by catalysed CVD on silicon oxide substrates, as this process produces clean SWNTs without the need for further processing, directly on an insulating substrate, with controllable surface coverage [42, 43] (*vide infra*). In this configuration SWNTs are the electrode element. The results are compared against those obtained using commercial SPCEs. Finally, after identification of the most effective SWNT density, for low concentration detection with minimal fouling, we produce and demonstrate a user-friendly SWNT 3-electrode format for electroanalysis, akin to that found with SPCE platforms. Our SWNT device contains a SWNT working electrode and SWNT counter electrode on a single planar chip, onto which a quasi-silver reference electrode is evaporated.

Experimental

Chemicals and solutions

All chemicals were used as received. Aqueous solutions were prepared using deionized water produced by a Purite Select HP system (resistivity of 18.2 M Ω cm at 25 °C). FcCOOH (VWR International Ltd., 98 %) was prepared in 8 % (weight/weight (*w/w*)) of PEG 2K (VWR International Ltd., UK) and 0.01 M phosphate-buffered solution (PBS, pH 7). PBS was prepared in-house from sodium phosphate dibasic heptahydrate (Na₂HPO₄·7H₂O, Sigma-Aldrich, 98 – 100 %, UK) and sodium dihydrogen orthophosphate dihydrate (NaH₂PO₄·2H₂O, Fisher Scientific, 99 – 100 %, UK). 4 % (*w/w*) albumin (Sigma-Aldrich, 97 %, UK) electrolyte was prepared in 0.01 M PBS.

Electrode materials

SPCE. Figure 1a shows a schematic of a 3-electrode SPCE (Kanichi Research, UK), consisting of a 3 mm diameter graphite disk as the working electrode (WE), a hemispherical band of graphite as the counter electrode (CE) and a quasi Ag/AgCl reference electrode (RE), printed onto polyvinyl chloride.

Controlled growth of SWNT Networks: SWNT networks were grown on 2 cm × 2 cm silicon (Si) substrates with 300 nm of thermally grown silicon oxide (SiO₂: IDB Technologies Ltd., n-type, 525 μ m thick Si) using cCVD. Iron nanoparticles (Fe NPs) were used as catalysts [14] for the growth of low density (LD) networks, whereas cobalt (Co) NPs were employed as catalysts [44] for both high density (HD) and super HD (SHD) networks. Fe NPs were deposited by soaking the Si/SiO₂ substrate in 1 % ferritin (50 – 150 mg mL⁻¹, Aldrich, UK) aqueous solution for 1 hour, followed by a 2 min exposure to a 100 W oxygen plasma (Emitech K1050X plasma asher, UK). Co was deposited by sputtering (SC7640 sputter coater, Quorum Technologies Ltd., UK) at 1 kV for 20 s and 30 s, respectively, for the growth of HD and SHD SWNT networks.

Patterned SHD SWNTs: A Kapton film mask compatible in size with a 1.7 cm × 2 cm Si/SiO₂ substrate, was prepared using laser micromaching (Oxford Lasers Ltd. E-355H-3-ATHI-O). The laser system was equipped with a Q-switched fully diode-pumped solid state Nd:YAG laser medium with a primary output wavelength of 355 nm. Specifically, an area of 0.1 cm by 1.5 cm was exposed for the WE and 0.2 cm by 1.5 cm for the CE. Co NP catalyst deposition was carried out as described above and then the Kapton film mask was removed.

SWNT Growth: The Si/SiO₂ substrate was heated from room temperature to 850 °C over a period of 14 min under H₂ (BOC Gases, 99.95 %, UK) atmosphere at a flow rate of 150 sccm, followed by 1 min stabilization at 850 °C. The carbon feedstock, ethanol (Fisher, 99.99 %, UK) was then introduced via a flow of Ar (BOC Gases, 99.9995 % UK) (850 sccm) held at 0 °C. Growth was carried out for 10, 20 and 30 mins for low density (LD), high density (HD) and super high density (SHD) SWNT networks, respectively. The system was left to cool under H₂ gas. Electrical contact to the SWNT networks was achieved by evaporating a band at one edge, of Cr (3 nm) followed by Au (60 nm). For the patterned electrode, Ag (60 nm) was evaporated through a shadow mask, using a Moorfields MiniLab deposition system (Moorfield Associates, UK), to form both a 0.1 × 1.5 cm quasi Ag RE and an electrical contact to the SWNT WE (0.1 cm × 0.6 cm) and CE (0.2 cm × 0.6 cm). Figures 1b and 1c respectively show the unpatterned and patterned SWNT network electrodes.

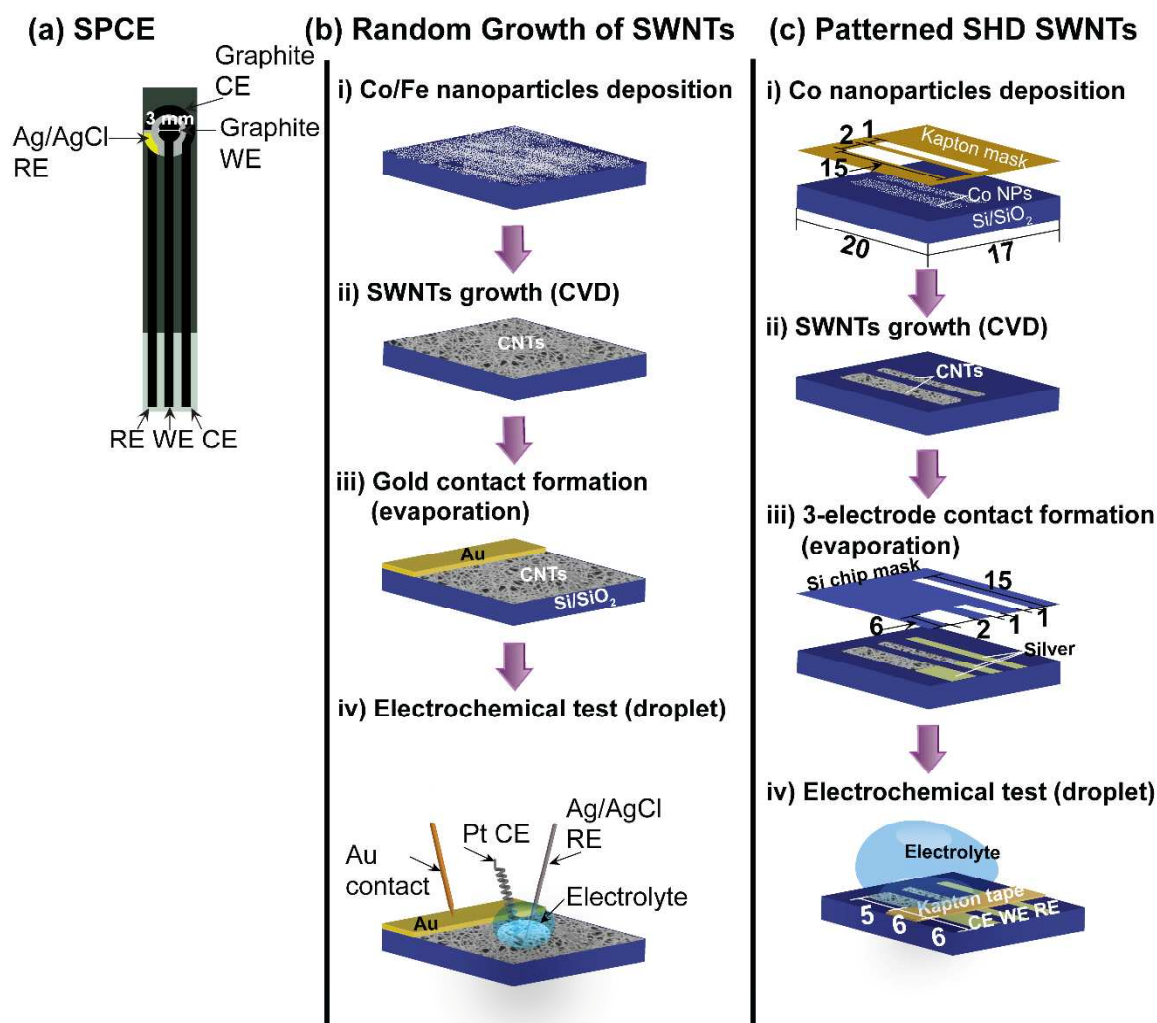


Figure 1: Schematic of the different 3-electrode arrangements employed: (a) SPCE. (b) Network SWNTs on an insulating surface produced by i) catalyst deposition, ii) SWNT growth, iii) gold contact for the SWNT working electrode, iv) outlines the experimental arrangement for electrochemical measurements. (c) SWNT patterning processes to produce a SWNT electrochemical device on an Si/SiO₂ substrate showing i) catalyst NP deposition, ii) SWNT growth via CVD, iii) electrode contact and Ag quasi RE formation using evaporation and iv) the electrochemical droplet method. The unit of length for all numerical labels is mm.

SWNT network and SPCE characterization

Field emission scanning electron microscopy (FE-SEM) images were acquired ($n = 3$) using a Zeiss Supra 55-VP at 1 kV acceleration voltage to visualize the SWNT networks with different

densities and the microstructure of SPCEs. Micro-Raman spectra were recorded using a Renishaw inVia Raman microscope (514.5 nm Ar laser, 10 mW, $n = 3$).

Electrochemical experiments

To perform droplet measurements in the configuration of Figure 1b (iv), SWNT networks were connected as the WE. A drop of electrolyte solution ($\sim 15 \mu\text{L}$, 4 mm diameter) containing FcCOOH mediator and 0.01 M PBS was placed on the electrode surface, close to the Au band but without making contact with it. An AgCl-coated Ag wire acted as a quasi-RE and a platinum wire was used as a CE. Both were carefully positioned within the drop of solution to complete the 3-electrode arrangement. The electrochemically active area of the SWNT patterned electrode, was defined using kapton tape ($1.7 \text{ cm} \times 0.6 \text{ cm}$), resulting in ca. 0.05 cm^2 area for the WE, 0.1 cm^2 for the CE and 0.05 cm^2 for the RE. A drop of solution containing redox mediator and supporting electrolyte was placed on the surface, so as to cover all 3 electrodes (Figure 1c (iv)).

EC measurements were conducted using a CH Instruments (Austin, TX; model 1040A) potentiostat. CV and differential pulse voltammetry (DPV) were used for the EC measurements. DPV scans were recorded at 50 ms pulse width, 20 mV potential step, 200 ms pulse period with an potential amplitude of 50 mV. All EC measurements were carried out without a Faraday cage.

Results and discussion

SWNTs networks of controlled surface coverage

All SWNT networks in this study had a connectivity greater than the metallic percolation threshold ($\rho_{th(\text{metallic})}$), $1.4 - 2.4 \mu\text{m}_{\text{SWNT}} \mu\text{m}^{-2}$; based on typical SWNTs lengths of $7 - 12 \mu\text{m}$

with sufficient metallic (m)SWNT to mSWNT connections to act as an electrode material.[28] cCVD growth typically results in 1/3rd of the SWNTs with metallic characteristics, the remaining 2/3rd are semiconducting (p-type) [45, 46]. Figure 2a shows a typical FE-SEM image of a LD SWNT network, which has a density of $5 (\pm 1) \mu\text{m}_{\text{SWNT}} \mu\text{m}^{-2}$. For HD and SHD SWNTs, it is difficult to accurately determine the network density using FE-SEM owing to the aggregation of individual SWNT to bundles. This is evidenced by the obvious layering of CNTs with the increase of SWNT density (Figure 2b and c). The surface morphology of a SPCE is illustrated in Figure 2d showing the significant heterogeneity of the surface.

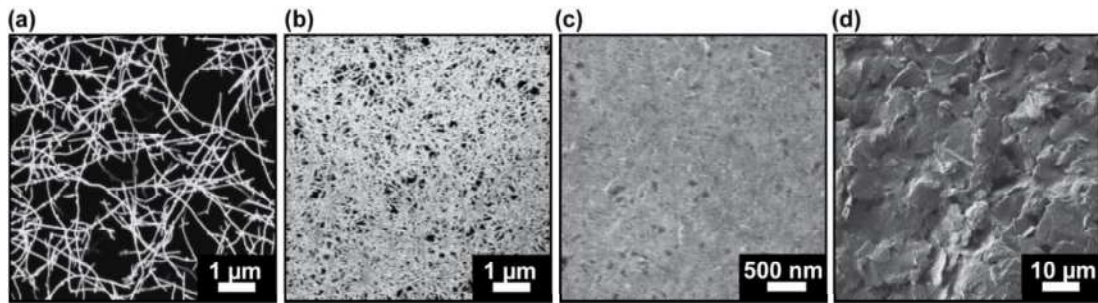


Figure 2: Typical FE-SEM images of (a) LD, (b) HD, (c) SHD SWNT networks, and (d) SPCE.

Due to the aggregation of SWNTs for the HD and SHD electrodes, the network density was instead estimated from the double layer capacitance, as the non-faradaic current would be reasonably expected to scale with the density of SWNTs. CVs (scan rate 100 mV s^{-1}) of the LD, HD and SHD SWNT network electrodes, and the SPCE in supporting electrode (0.01 M PBS) are shown in Figure 3 and the calculated capacitance values are summarized in Table 1. The specific capacitance values, C , of $60 \pm 5 \text{ nF cm}^{-2}$ (LD SWNT); $280 \pm 15 \text{ nF cm}^{-2}$ (HD SWNT); $400 \pm 30 \text{ nF cm}^{-2}$ (SHD SWNT) and $8600 \pm 100 \text{ nF cm}^{-2}$ (SPCE) were calculated from CVs presented in Figure 3, at 0 V versus Ag/AgCl in 8 % PEG 2K + 0.01 M PBS, using:

$$C = \frac{i_{\text{average}}}{vA_{\text{geometric}}} \quad (1)$$

where i_{average} is the average current magnitude of the forward and reverse sweep, ν is the scan rate and $A_{\text{geometric}}$ is the geometrical area of the electrode. It is worth noting that the specific capacitances of the SWNT networks are $\times 20$ (SHD), $\times 30$ (HD) and $\times 140$ (LD) lower than that of the SPCE. The HD SWNT network (Figure 2b) thus had an estimated density of $\sim 20 \mu\text{m}_{\text{SWNT}} \mu\text{m}^{-2}$ calculated from the specific capacitance while the SHD SWNT network (Figure 2c) had an estimated density of $\sim 30 \mu\text{m}_{\text{SWNT}} \mu\text{m}^{-2}$.

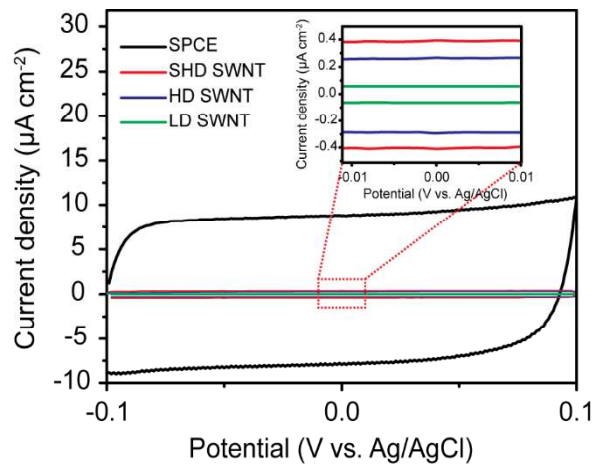


Figure 3: CVs for specific capacitance measurement in 8 % PEG 2K + 0.01 M PBS (100 mV s^{-1}) on SPCE (black), SHD (red), HD (blue) and LD (green) SWNT networks.

Figure 4 shows representative micro-Raman spectra of LD, HD, and SHD SWNT networks and SPCE, with the wavenumber ranging from 100 to 2600 cm^{-1} . For the SWNT networks, the peaks marked with (*) at 303 cm^{-1} , 521 cm^{-1} and 963 cm^{-1} originate from the Si/SiO₂ substrate and serve as a reference against which other peaks can be compared. In all spectra the presence of the G peak (1585 cm^{-1}) indicates sp² carbon [47] and radial breathing modes[48] (RBM, 100 to 350 cm^{-1}) positively identify the networks as SWNTs. It is clear that the intensity of the G peak increases with the increased density of SWNTs in resonance with the Raman laser (*vide supra*). [48] The D peak at 1350 cm^{-1} originates from sp³ carbon which can be found at defects or is due to amorphous carbon [49]. The intensity difference of the G peak to D peak is used as an indicator of the quality of SWNTs [50]. The G peak was *ca.* $\times 40$, $\times 30$ and $\times 20$ the

intensity of *D* peak for the LD, HD and SHD network SWNTs, respectively, confirming the high quality of the as-grown SWNTs, which have low intrinsic defect densities. In contrast, the *D* peak intensity of the SPCE is comparable with that of *G* peak which is possibly due to amorphous carbon and the binder that covers the SPCE surface [51]. Note, due to resonance effect of the excitation energy and the absorption bands of SWNTs, the Raman count signal is much higher for SWNTs than for the SPCE [52].

Table 1 Estimated values of the network density from specific capacitance of SWNT network electrodes and comparison to SPCE

| Electrode | Specific capacitance (nF cm ⁻²) | SWNT density estimated from specific capacitance (μm _{SWNT} μm ⁻²) |
|-----------|---|---|
| LD SWNT | 600 ± 5 | 5 ± 1 (determined from FE-SEM presented in Figure 2a) |
| HD SWNT | 2800 ± 15 | ~ 20 |
| SHD SWNT | 4000 ± 30 | ~ 30 |
| SPCE | 86000 ± 100 | Not applicable |

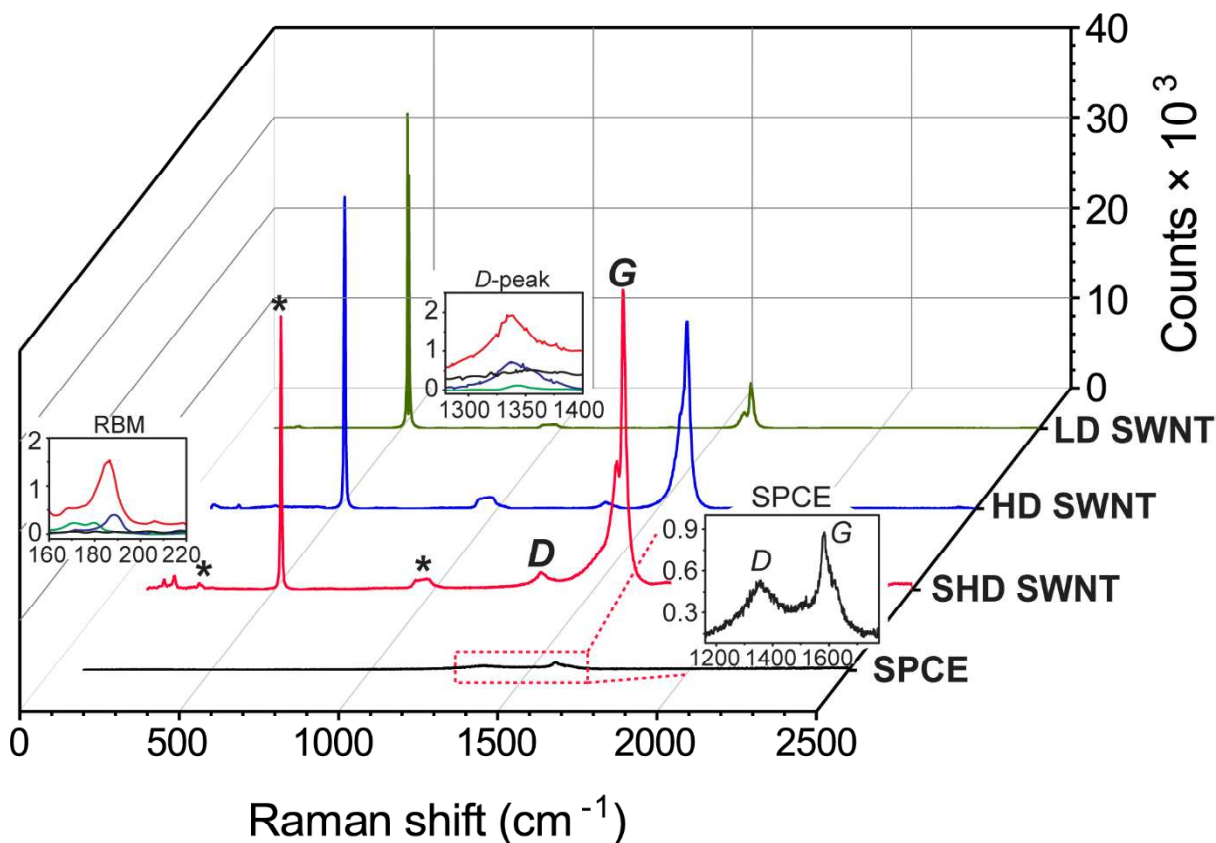


Figure 4 Micro-Raman spectra of SPCE (black), SHD (red), HD (blue) and LD (green) SWNT networks.

CV response and detection limit of FcCOOH for LD, HD, SHD SWNT network electrodes compared to SPCEs

CV was initially employed to analyze the detection sensitivity of FcCOOH oxidation at the three different SWNT network density electrodes and SPCEs, in a PEG-containing solution. The increased viscosity of the 8% PEG 2K solution results in a decrease of the diffusion coefficient for FcCOOH from $5.20 \times 10^{-6} \text{ cm}^2 \text{ s}^{-1}$ to $3.50 \times 10^{-6} \text{ cm}^2 \text{ s}^{-1}$, supporting information, S1. Figure 5 shows typical CVs recorded over the FcCOOH concentrations range 15 nM – 100 μM in 8% PEG 2K (w/w) and 0.01 M PBS, at a scan rate of 100 mV s^{-1} . Note that the current density is calculated based on the geometric area of each electrode device. The CVs in Figure 5a recorded on a LD SWNT network show a linear dependence of peak current (i_p) on

concentrations in the range 15 to 100 nM (inset) for the oxidation of FcCOOH. Even at 25 nM FcCOOH the oxidative current signal is easily discernible. The ability to distinguish such low concentrations voltammetrically, using the LD SWNT network is attributed to the very low intrinsic background current. This results from the significantly low density of SWNTs, as seen previously for solutions that did not contain possible adsorbing additives [27].

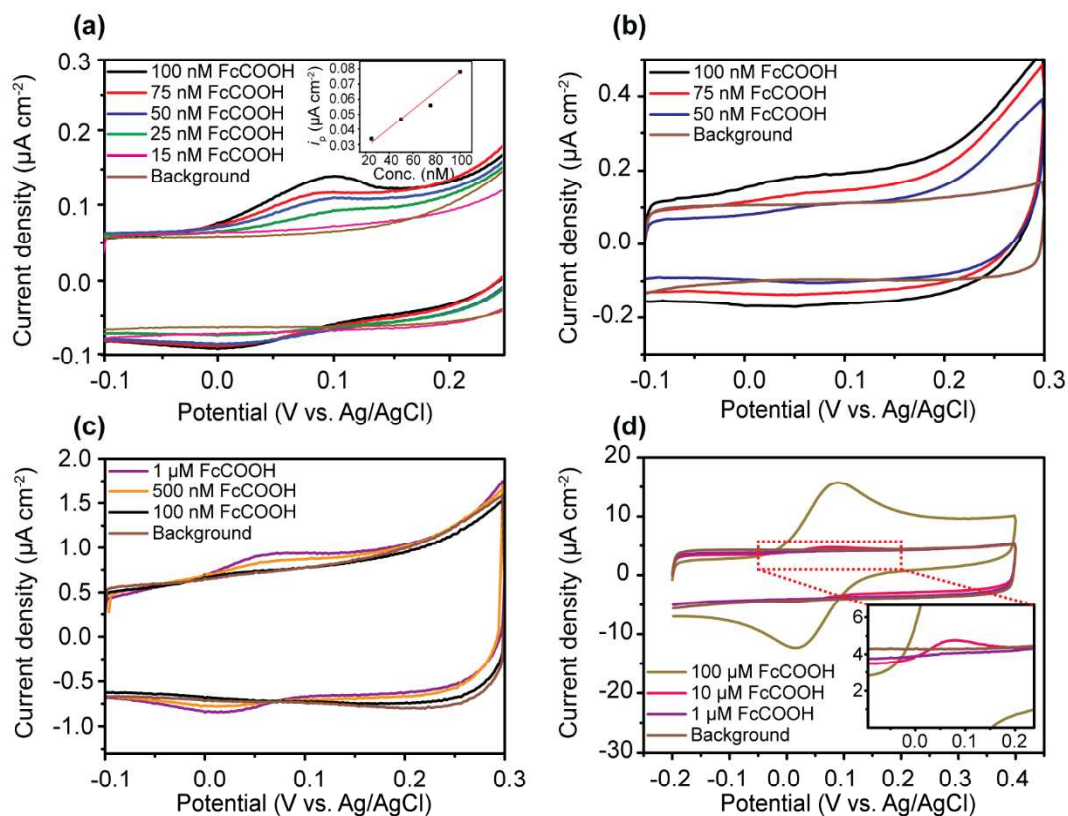


Figure 5 CVs for the oxidation of different concentrations of FcCOOH in 8% PEG 2K and 0.01 M PBS (100 mV s^{-1}) at (a) LD (Inset is the plot of i_p vs. Concentration), (b) HD, (c) SHD SWNT networks and (d) SPCE.

At the HD SWNT network electrode, a detectable redox current is observed for concentrations $\geq 75 \text{ nM}$ FcCOOH (Figure 5b), while for the SHD SWNT network electrode, this value is $\geq 500 \text{ nM}$ (Figure 5c). This behaviour is expected, as the capacitive background current scales with the SWNT network density which impairs the detection limit. Further capacitive

constraint was observed at SPCEs with a detectable concentration value which is significantly higher, $\geq 10 \mu\text{M}$ FcCOOH (Figure 5d).

The peak to peak separation (ΔE_p) for FcCOOH on the different electrodes was 62 mV (100 nM; HD SWNT), 60 mV (1 μM ; SHD SWNT) and 72 mV (100 μM ; SPCE), values which are reasonably close to reversible behaviour. This indicates facile ET kinetics for this one-electron oxidation, noting that the droplet arrangement is more prone to ohmic effects [53], which could influence the data with 100 μM and higher FcCOOH concentration. However, ΔE_p for the LD SWNT network at 100 nM FcCOOH is 90 mV. The larger ΔE_p value could be due to this network having the highest intrinsic resistance of all three networks, although we note that very small currents are passed. More likely, the apparent reduction in electrochemical kinetics is due to the LD network having a greater susceptibility to blocking effects (attachment of PEG molecules to the surface), *vide infra*. Here the interplay between the electrochemical kinetics and the (already high) local diffusional flux at sparse SWNTs [54] will be pushed towards increasing apparent kinetic constraint by any further passivation of the SWNT surface.

DPV response of LD, HD, SHD SWNT network electrodes and SPCE

DPV was employed as a means of improving the detection sensitivity [55], focusing on the oxidation of FcCOOH in 8% PEG 2K solutions. As shown in Figure 6, the lowest detectable concentration was greatly improved for all electrodes, with concentrations of 5 nM for the LD SWNT (Figure 6a), 5 nM for the HD SWNT (Figure 6b), 1 nM for SHD SWNT (Figure 6c) now resolvable. The resulting peak current versus concentration plots were linear for all four electrodes, resulting in limits of detection (LOD) of 1.30 ± 0.01 nM (LD), 1.05 ± 0.04 nM (HD), 1.00 ± 0.003 nM (SHD) and $2.05 \pm 0.06 \mu\text{M}$ (SPCE), Supporting Information S2. This result is very interesting in that it shows that for the SWNT networks, irrespective of density,

a similar LOD results, at the 1 nM level, when a potential pulse sequence is used to collect the data. Moreover, all three SWNT electrodes give a quantitative response to a concentration of FcCOOH that is *ca.* 1000 times lower than that obtained from the SPCE.

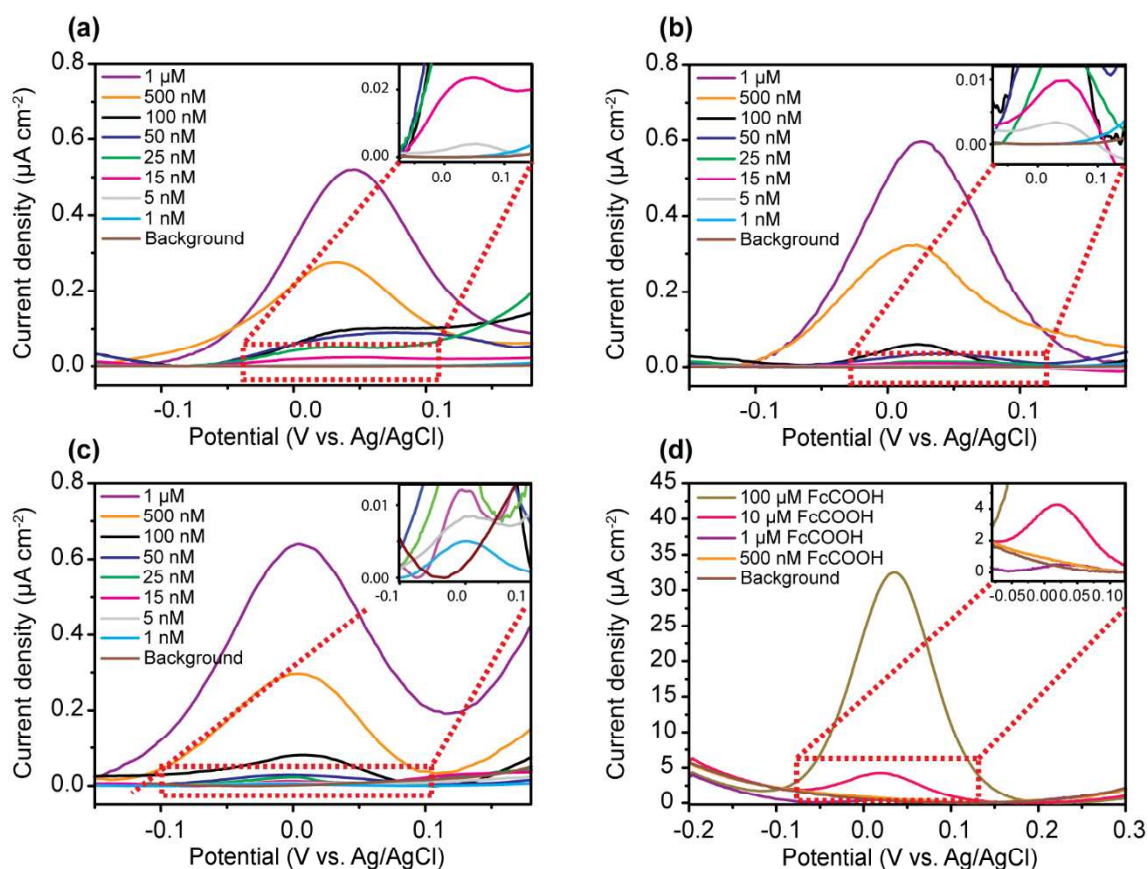


Figure 6 DPVs for the oxidation of different concentrations of FcCOOH in 8% PEG 2K and 0.01 M PBS at (a) LD, (b) HD, (c) SHD SWNT networks and (d) SPCE. Inset is a zoom-in to a particular region of the DPVs.

DPV, and other potential pulse techniques such as square wave voltammetry, decrease the detectable concentration by collecting currents in a region of the current-time curve (for each potential pulse) where the non-faradaic current has decayed to zero [56]. Under ideal conditions, the non-faradaic response will be controlled only by uncompensated resistance and double layer capacitance effects (RC). If the system suffers from high R or C contributions already, it may be difficult to sample the current under conditions where the non-faradaic

contribution has decreased to zero, due to the high time constant. Moreover, if pseudo-capacitive contributions are present, e.g. due to the presence of redox active molecules on the surface, such as quinone groups, an additional faradaic contribution will arise which cannot be negated using DPV, SWV etc [56].

The results observed indicate that the RC component in the SWNT electrode system is small, even when the C is larger for the higher density electrodes. The cleanliness, low defect density and minimal levels of amorphous carbon of SWNTs grown by CVD, results not only in low values for the double layer capacitance per length of SWNT [57], but means there are unlikely to be any redox active groups on the SWNT surface. In contrast, the SPCE, which possesses by far the highest capacitive current, did not yield a particularly low detection limit (μM range) due to the complexity of the graphitic surface, composed of organic oil, binder paste and the presence of other surface redox groups (such as surface-bound quinones) [8, 10].

Fouling Effects of Additives

To investigate the fouling effect of additives, either PEG 2K [58] or albumin [29] was added to the analyte solution [59, 60] and the CV cycled fifteen times. Figure 7 shows 14 repeat cycling CVs (starting from the 2nd CV) for $100 \mu\text{M}$ FcCOOH oxidation in 8% (w/w) PEG 2K on SWNT networks of LD (Figure 7a), HD (Figure 7b), SHD (Figure 7c) and SPCE (Figure 7d). As the CVs were cycled continuously, and no wait time implemented, we show only the CVs starting from the second scan due to the possible contribution of analyte depletion effects which will be felt most severely from the first to second scan (first CV cycle for each run is in Supporting Information, S3).

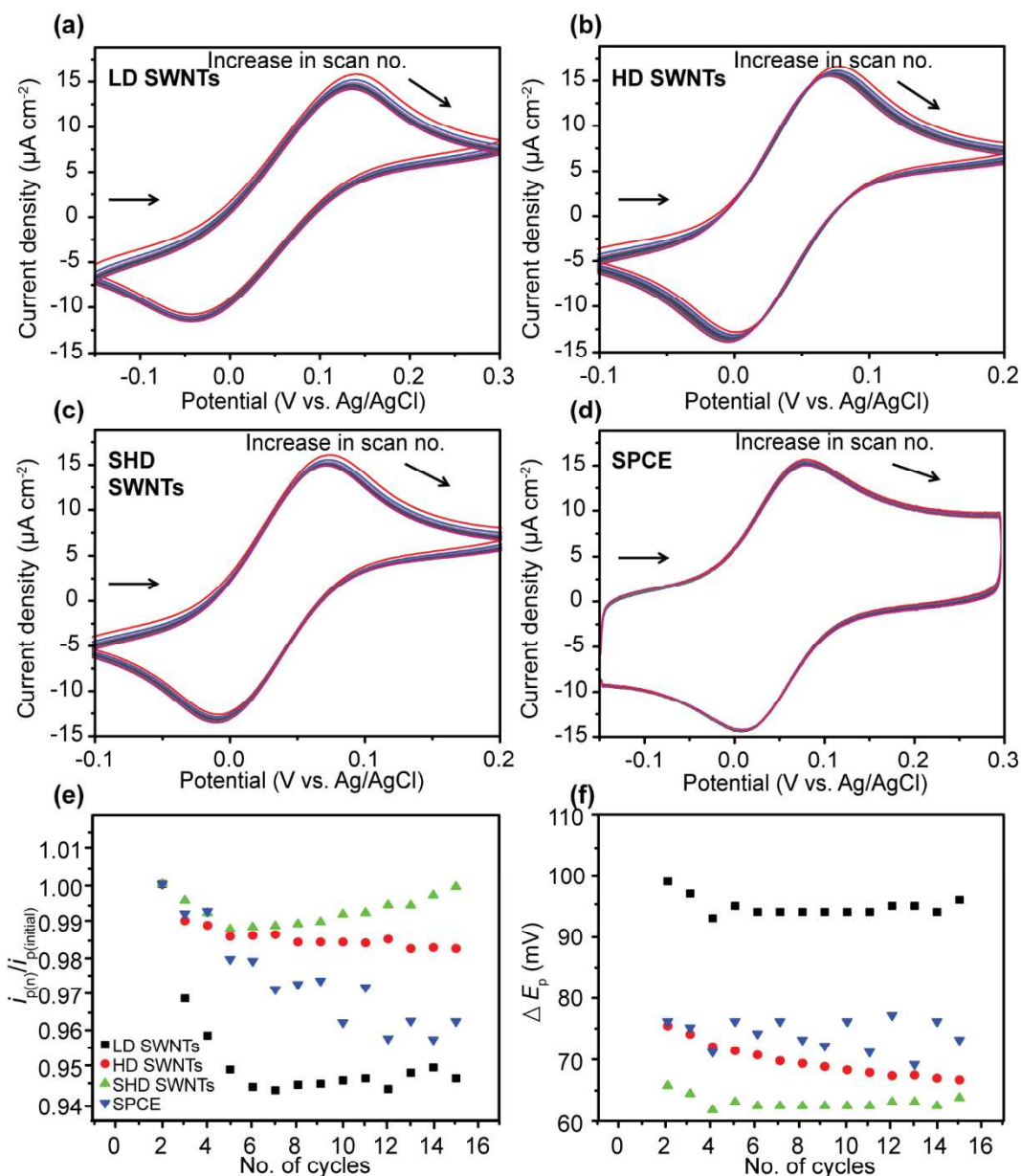


Figure 7: CVs of 14 consecutive cycle from the second scan for the oxidation of 100 μM FcCOOH in 8 % PEG 2K and 0.01 M PBS at (a) LD, (b) HD, (c) SHD SWNT networks and (d) SPCE, scan rate 100 mV s^{-1} . (e) $i_{p(n)}/i_{p(\text{initial})}$ versus number of scan cycles (f) ΔE_p versus number of scan cycles.

Figure 7e shows summary data of i_p normalised by the value on the second scan as a function of number of CV cycles. i_p typically decreases with consecutive scans, with the extent depending on SWNT coverage and type of carbon electrode. It is obvious from Fig. 7a that the

LD SWNT networks appear to be more susceptible to fouling than the other electrodes, with a drop in the FcCOOH oxidative peak current, i_p by 5.2 % after fourteen CVs compared to an i_p drop of 2 % for HD SWNTs (Fig. 7b), 0.2 % for SHD SWNTs (Fig. 7c) and 4.6 % for SPCE (Fig. 7d). Figure 7f shows the summary data of ΔE_p as a function of number of CV cycles. There is a small decrease in ΔE_p with consecutive scans for all SWNT network densities, whilst ΔE_p remains fairly constant over the 14 consecutive scans for SPCE (73 ± 5 mV). The apparent faster electrochemical kinetics, and smaller observed decreases in i_p with increasing scan number, for the higher density SWNT networks, is attributed to the higher surface coverage of SWNTs. With a high density of active material, and contrary to the discussion on the LD SWNT above, changes to FcCOOH mass transport per unit area of SWNT, as a result of SWNT blocking, will be less strongly felt as the rate of redox-reaction per unit area of active electrode material is much lower.

The effect of albumin in solution was investigated in a similar fashion using 100 μ M FcCOOH and 4 % albumin (*w/w*), with CV data shown in Figure 8. Again, the response of the LD SWNT network is more susceptible to fouling than the other electrodes, as judged by the diminution in CV response, with a drop in i_p by 14 % (Figure 8a), compared to 4 % (HD SWNT network; Figure 8b), 3.8 % (SHD SWNT network; Figure 8c) and 7 % (SPCE; Figure 8d) over fourteen scans.

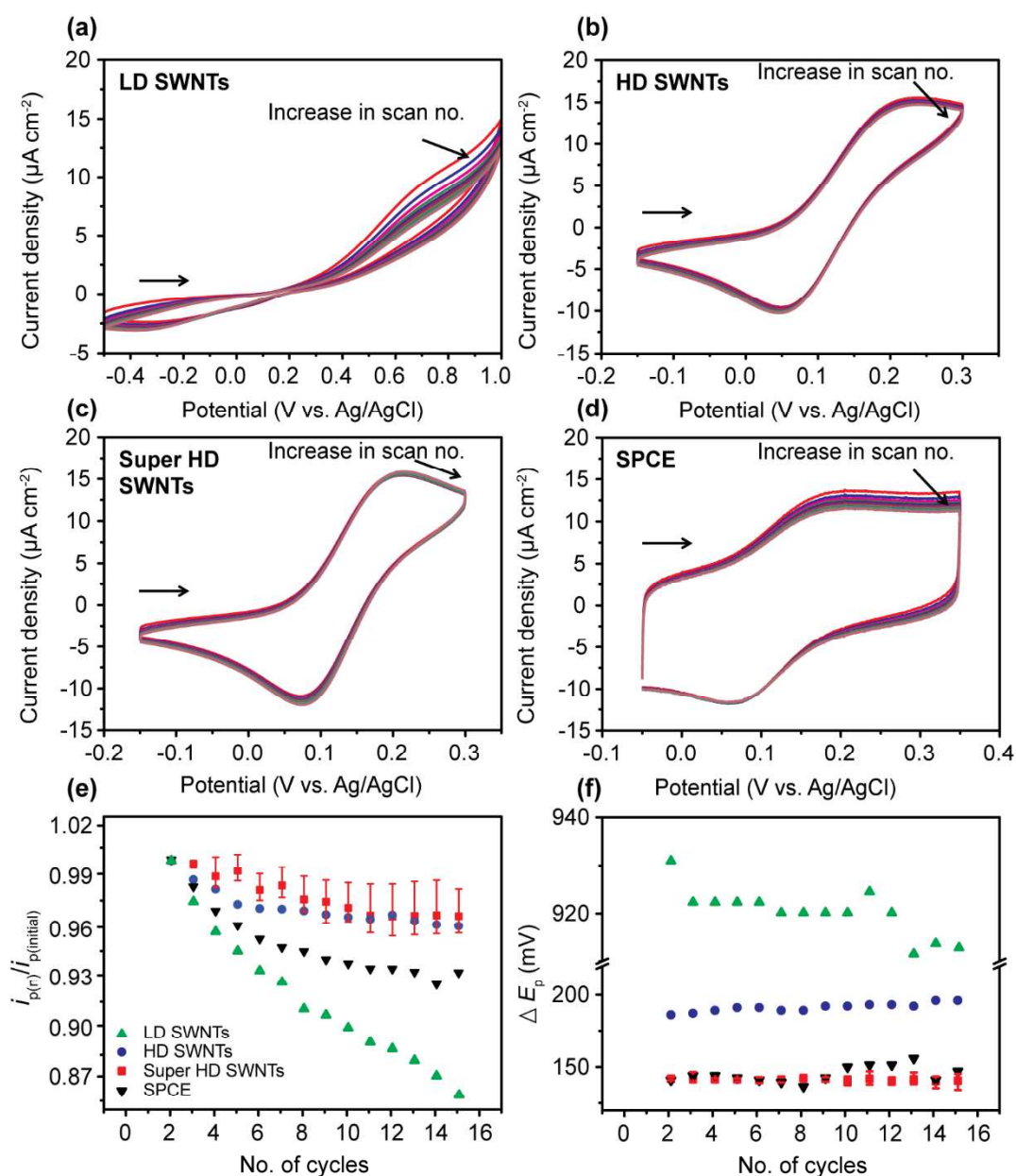


Figure 8 CVs of 14 consecutive cycles for the oxidation of 100 μM FcCOOH in 4 % albumin and 0.01 M PBS at (a) LD, (b) HD, (c) SHD SWNT networks and (d) SPCE, scan rate 100 mV s^{-1} . (e) $i_{p(n)}/i_{p(\text{initial})}$ versus number of cycles (with the initial value taken from the second cycle – see text) and (f) ΔE_p versus number of cycles: SPCE (black), SHD SWNTs (red), HD SWNTs (blue), and LD SWNT networks (green).

Interestingly, the HD and SHD SWNT networks exhibit good stability with little change in i_p . The redox behaviour of FcCOOH for the SHD SWNT networks shows an average ΔE_p value

of 140 ± 10 mV (2nd to 15th cycle), the value for the HD SWNT networks is 170 ± 10 mV whilst that for the LD SWNT network is 920 ± 15 mV. The increased ΔE_p in albumin compared to that in PEG 2K indicates apparently slower kinetics, attributed to stronger adsorption of albumin on the electrode surfaces. The SPCE shows a ΔE_p of 140 ± 10 mV similar to that of SHD SWNT networks.

Controllable preparation of a high density SWNT three-electrode cell

Based on the data above, both HD and SHD SWNT networks show promise as electroanalytical detectors in media that mimic biological environments. To this end, SWNT devices with a format similar to that of the SPCE, i.e. with WE, RE and CE tracks all on the same insulating substrate (chip) were prepared and tested electrochemically. A HD SWNT network (~ 20 μm length of SWNT per μm^2) was used for these studies.

The photograph in Figure 9a shows the 3-electrode design, with the lithographically-defined HD SWNT network electrodes for the WE and CE, and a quasi-Ag electrode for the RE. Figure 9b shows a typical FE-SEM image of the 1 mm width HD SWNT network band on the inert Si/SiO₂ substrate, whilst Figure 9c is a higher resolution FE-SEM of the multiply-interconnected and randomly oriented SWNT networks. Figure 9d shows representative micro-Raman spectra of the HD SWNT network ranging from 100 to 2500 cm^{-1} . The *G* peak was *ca.* 30 \times the intensity of the *D* peak for HD SWNT network, indicating that the as-grown HD SWNTs have low intrinsic defect densities, matching well with the data in Figure 4.

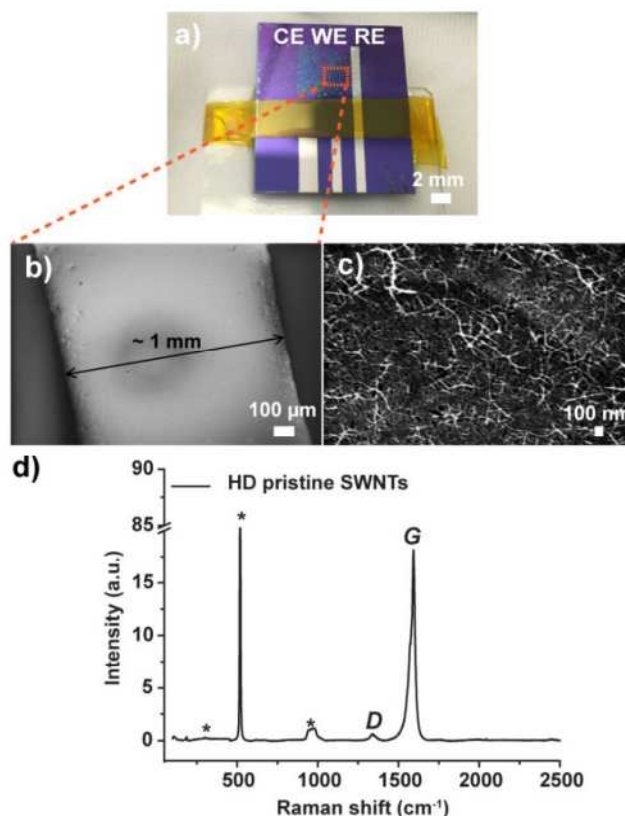


Figure 9 (a) Photograph of the 3-electrode SWNT patterned device. (b) FE-SEM image of 1 mm width SWNT network grown on the inert substrate acting as WE; (c) zoom of SWNT network. (d) Micro-Raman spectrum of SWNTs in the device.

Electrochemical characterisation of three-electrode SWNT chip using DPV

To demonstrate the electrochemical viability of the 3-electrode SWNT chip, a small volume of analyte solution (5 μL) was placed on the device and DPV employed for electroanalysis. Figure 10a shows typical DPVs recorded at different concentrations of FcCOOH (25 nM (red), 50 nM (blue), 100 nM (magenta), 500 nM (olive), 1 μM (navy), and 5 μM (violet)) in 8 % PEG (w/w) and 0.01 M PBS (black). The response of 25 nM (red) is easily visible at the SHD SWNT network electrode (Figure 10b). Figures 10c and d show the plot of peak currents as a function of FcCOOH concentrations (25 nM to 5 μM) in 8% PEG 2K and 0.01 M PBS. The peak current increased linearly with FcCOOH concentration, with a gradient of $0.33 \pm 0.01 \text{ A cm}^{-2} \text{ M}^{-1}$ (R^2

= 0.99468) and a detection limit of 6.6 ± 0.2 nM for HD SWNTs. This data is in fairly good agreement with the lowest detectable concentration shown for the HD network operating in a droplet cell configuration, Figure 6b.

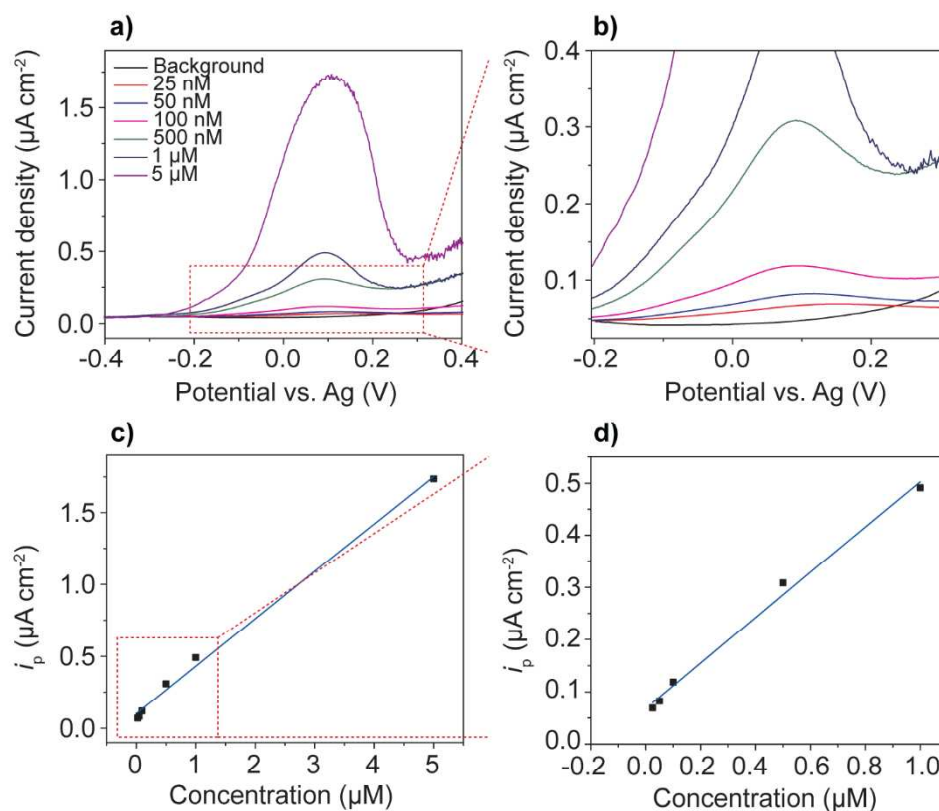


Figure 10. Electrochemistry at a HD SWNT 3-electrode chip. (a) Typical DPVs for the oxidation of different concentrations of FcCOOH (25 nM to 5 μM) in 8% PEG 2K and 0.01 M PBS. (b) Zoom of DPV curves to highlight the response of the lowest FcCOOH concentrations. (c) Plot of i_p versus concentration of FcCOOH and (d) magnification of the low concentration range.

Conclusions

SWNT network electrodes have been demonstrated to be very effective for trace level detection voltammetric measurements in both PEG and albumin-containing aqueous media. SWNT network electrodes outperform SPCEs in terms of lowest detectable concentration, by up to

three orders of magnitude, in the presence of a model electroactive analyte, FcCOOH. Both CV and DPV were employed to study this redox reaction at commercial SPCEs and SWNT network electrodes covering a range of network densities from low, LD = 5 (± 1) $\mu\text{m}_{\text{SWNT}} \mu\text{m}^{-2}$, to high HD $\sim 20 \mu\text{m}_{\text{SWNT}} \mu\text{m}^{-2}$ to superhigh (SHD) $\sim 30 \mu\text{m}_{\text{SWNT}} \mu\text{m}^{-2}$.

Using CV, in 8% PEG 2K solutions, the lowest detectable concentration for FcCOOH decreased as the network density decreased. Interestingly, with DPV, which acts to remove non-faradaic contributions, the lowest detectable concentration was found to be relatively independent of network density, with all three networks giving a FcCOOH limit of detection of 1 nM. This value was three orders of magnitude lower than achievable with SPCEs (1 μM) and was attributed to the cleanliness of the SWNTs grown via CVD, resulting in low capacitive currents and absence of amorphous carbon which can contribute a pseudo-capacitive (faradaic) response.

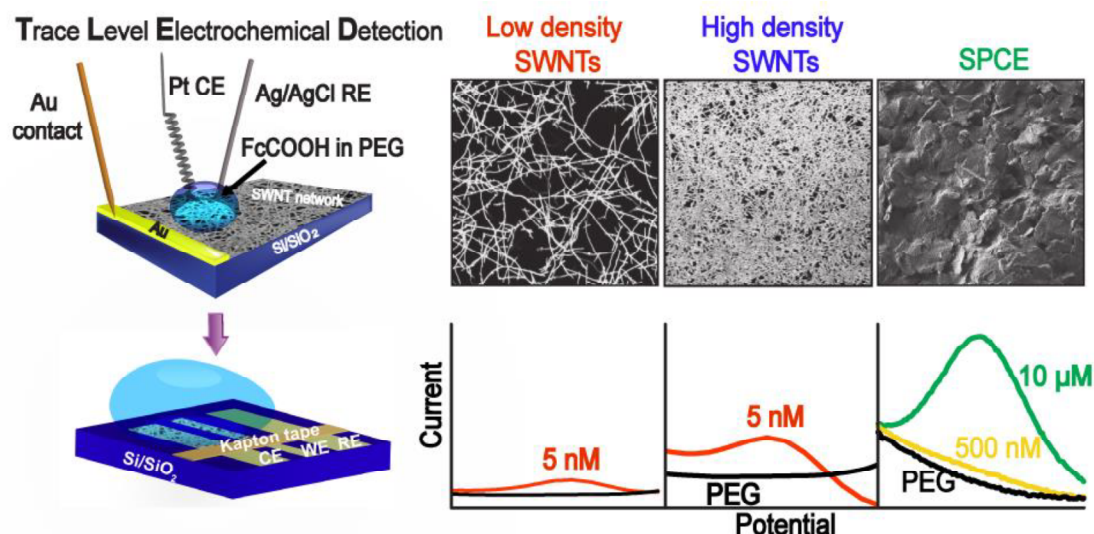
Repeat cycling (fifteen cycles in total) of the three different density SWNT network electrodes in FcCOOH solutions containing either 8% PEG 2K or albumin, showed that the LD networks suffered the most from fouling effects, impairing the electrochemical response and detection sensitivity. The SPCE showed some fouling effects, but not as significant as the LD SWNT electrode, while the response of the HD and SHD SWNT electrodes indicated they were relatively immune to fouling. This trend is due to the interplay between mass local transport-surface fouling and intrinsic electrochemical kinetics of the SWNTs. For LD SWNTs, the local high mass transport (flux) is very high, which places greater apparent kinetic demands on the active part of the electrode, and hence a greater sensitivity of the response to any blocking effects, which is much less significant for higher coverage SWNT devices. Thus, both HD and SHD network electrodes are suitable for trace voltammetric applications in biological media.

Finally, a lithographic patterning procedure was used to produce SWNT-based electrode devices (chips) which mimic that of the commercial SPCE. The WE and CE comprised of HD SWNT networks whilst the RE was evaporatively deposited Ag. The HD SWNT network showed a detection limit for FcCOOH of 6.6 nM in the presence of 8% PEG 2K. The SWNT network electrode platform paves the way for trace electrochemical measurements at carbon electrodes, in a ready-to-use format. Compared to SPCEs, this device offers greatly improved sensitivity and detection limits in the presence of additives which mimic those found in biological media.

Acknowledgements

The authors thank Dr. Yang-Rae Kim, Dr. Aleix G. Güell, and Dr. Ashley Page for their help and support. SPE thanks the University of Warwick for the funding through the award of Chancellor's International Scholarship. TSM acknowledges support from EPSRC for a PhD studentship. The Royal Society is acknowledged for a Wolfson Research Merit Award to PRU and an Industry Fellowship to JVM.

Insert Table of Contents Graphic and Synopsis Here



Comparison of single-walled carbon nanotube network and commercially available screen-printed carbon electrode for trace level electrochemical detection in biological media.

References

- [1] Y. Wang, Z.H. Li, J. Wang, J.H. Li, Y.H. Lin, Graphene and graphene oxide: biofunctionalization and applications in biotechnology, *Trends Biotechnol.*, 29 (2011) 205–212. <https://doi.org/10.1016/j.tibtech.2011.01.008>.
- [2] C.B. Jacobs, M.J. Peairs, B.J. Venton, Review: Carbon nanotube based electrochemical sensors for biomolecules, *Anal. Chim. Acta*, 662 (2010) 105-127. <https://doi.org/10.1016/j.aca.2010.01.009>.
- [3] J.N. Tiwari, V. Vij, K.C. Kemp, K.S. Kim, Engineered carbon-nanomaterial-based electrochemical sensors for biomolecules, *ACS Nano*, 10 (2016) 46-80. <https://doi.org/10.1021/acsnano.5b05690>.
- [4] M. Dequaire, A. Heller, Screen printing of nucleic acid detecting carbon electrodes, *Anal. Chem.*, 74 (2002) 4370-4377. <https://doi.org/10.1021/ac025541g>.
- [5] T.S. Mann, S.R. Mikkelsen, Antibiotic susceptibility testing at a screen-printed carbon electrode array, *Anal. Chem.*, 80 (2008) 843-848. <https://doi.org/10.1021/ac701829c>.
- [6] S.A. Wring, J.P. Hart, L. Bracey, B.J. Birch, Development of screen-printed carbon electrodes, chemically modified with cobalt phthalocyanine, for electrochemical sensor applications, *Anal. Chim. Acta*, 231 (1990) 203-212. [https://doi.org/10.1016/S0003-2670\(00\)86418-1](https://doi.org/10.1016/S0003-2670(00)86418-1).

- [7] C. Karuwan, A. Wisitsoraat, D. Phokharatkul, C. Sriprachuabwong, T. Lomas, D. Nacapricha, A. Tuantranont, A disposable screen printed graphene-carbon paste electrode and its application in electrochemical sensing, *RSC Adv.*, 3 (2013) 25792-25799. <https://doi.org/10.1039/C3RA44187C>.
- [8] J. Wang, B.M. Tian, V.B. Nascimento, L. Angnes, Performance of screen-printed carbon electrodes fabricated from different carbon inks, *Electrochim. Acta*, 43 (1998) 3459-3465. [https://doi.org/10.1016/S0013-4686\(98\)00092-9](https://doi.org/10.1016/S0013-4686(98)00092-9).
- [9] D. Martin-Yerga, A. Costa-Garcia, P.R. Unwin, Correlative voltammetric microscopy: structure-activity relationships in the microscopic electrochemical behavior of screen printed carbon electrodes, *ACS Sensors*, 4 (2019) 2173-2180. <https://doi.org/10.1021/acssensors.9b01021>.
- [10] R.C. Alkire, P.N. Bartlett, J. Lipkowski, *Electrochemistry of Carbon Electrodes*, Wiley, 2015.
- [11] F.N. Ishikawa, M. Curreli, C.A. Olson, H.I. Liao, R. Sun, R.W. Roberts, R.J. Cote, M.E. Thompson, C.W. Zhou, Importance of controlling nanotube density for highly sensitive and reliable biosensors functional in physiological conditions, *ACS Nano*, 4 (2010) 6914-6922. <https://doi.org/10.1021/nn101198u>.
- [12] Y.P. Song, H.F. Hu, M. Feng, H.B. Zhan, Carbon nanotubes with tailored density of electronic states for electrochemical applications, *ACS Appl. Mater. Inter.*, 7 (2015) 25793-25803. <https://doi.org/10.1021/acsami.5b07700>.
- [13] I. Dumitrescu, P.R. Unwin, J.V. Macpherson, Electrochemistry at carbon nanotubes: perspective and issues, *Chem. Commun.*, 45 (2009) 6886-6901. <https://doi.org/10.1039/B909734A>.

- [14] P.V. Dudin, P.R. Unwin, J.V. Macpherson, Electrochemical nucleation and growth of gold nanoparticles on single-walled carbon nanotubes: new mechanistic insights, *J. Phys. Chem. C*, 114 (2010) 13241-13248. <https://doi.org/10.1021/jp1043706>.
- [15] A.G. Güell, N. Ebejer, M.E. Snowden, K. McKelvey, J.V. Macpherson, P.R. Unwin, Quantitative nanoscale visualization of heterogeneous electron transfer rates in 2D carbon nanotube networks, *P. Natl. Acad. Sci. USA*, 109 (2012) 11487-11492. <https://doi.org/10.1073/pnas.1203671109>.
- [16] N.X. Viet, S. Kishimoto, Y. Ohno, Highly Uniform, Flexible microelectrodes based on the clean single-walled carbon nanotube thin film with high electrochemical activity, *ACS Appl. Mater. Interfaces.*, 11 (2019) 6389-6395. <https://doi.org/10.1021/acsami.8b19252>.
- [17] C.E. Banks, A. Crossley, C. Salter, S.J. Wilkins, R.G. Compton, Carbon nanotubes contain metal impurities which are responsible for the "electrocatalysis" seen at some nanotube-modified electrodes, *Angew. Chem*, 45 (2006) 2533-2537. <https://doi.org/10.1002/anie.200600033>
- [18] H.X. Luo, Z.J. Shi, N.Q. Li, Z.N. Gu, Q.K. Zhuang, Investigation of the electrochemical and electrocatalytic behavior of single-wall carbon nanotube film on a glassy carbon electrode, *Anal. Chem.*, 73 (2001) 915-920. <https://doi.org/10.1021/ac000967l>.
- [19] D. Paolucci, M. Marcaccio, C. Bruno, F. Paolucci, N. Tagmatarchis, M. Prato, Voltammetric quantum charging capacitance behaviour of functionalised carbon nanotubes in solution, *Electrochim. Acta*, 53 (2008) 4059-4064. <https://doi.org/10.1016/j.electacta.2007.10.007>.

- [20] G.L. Goh, S. Agarwala, Y.J. Tan, W.Y. Yeong, A low cost and flexible carbon nanotube pH sensor fabricated using aerosol jet technology for live cell applications, *Sens. Actuators B Chem.*, 260 (2018) 227-235. <https://doi.org/10.1016/j.snb.2017.12.127>.
- [21] J. Zhao, Y. Yu, B. Weng, W. Zhang, A.T. Harris, A.I. Minett, Z. Yue, X. Huang, J. Chen, Sensitive and selective dopamine determination in human serum with inkjet printed Nafion/MWCNT chips, *Electrochem. Commun.*, 37 (2013) 32-35. <https://doi.org/10.1016/j.elecom.2013.10.007>.
- [22] M.P. Pujadó, *Carbon Nanotubes as Platforms for Biosensors with Electrochemical and Electronic Transduction*, first ed. Springer Berlin Heidelberg, 2012.
- [23] K.I. Papadimitriou, C. Wang, M.L. Rogers, S.A.N. Gowers, C.L. Leong, M.G. Boutelle, E.M. Drakakis, High-performance bioinstrumentation for real-time neuroelectrochemical traumatic brain injury monitoring, *Front. Hum. Neurosci.*, 10 (2016) 212. DOI: 10.3389/fnhum.2016.00212.
- [24] I. Heller, J. Kong, H.A. Heering, K.A. Williams, S.G. Lemay, C. Dekker, Individual single-walled carbon nanotubes as nanoelectrodes for electrochemistry, *Nano Lett.*, 5 (2005) 137-142. <https://doi.org/10.1021/nl048200m>.
- [25] Y.W. Fan, B.R. Goldsmith, P.G. Collins, Identifying and counting point defects in carbon nanotubes, *Nat. Mater.*, 4 (2005) 906-911. DOI: 10.1038/nmat1516.
- [26] I. Dumitrescu, N.R. Wilson, J.V. Macpherson, Functionalizing single-walled carbon nanotube networks: Effect on electrical and electrochemical properties, *J. Phys. Chem. C*, 111 (2007) 12944-12953. <https://doi.org/10.1021/jp067256x>.

- [27] P. Bertoncello, J.P. Edgeworth, J.V. Macpherson, P.R. Unwin, Trace level cyclic voltammetry facilitated by single-walled carbon nanotube network electrodes, *J. Am. Chem. Soc.*, 129 (2007) 10982-10983. DOI:10.1021/ja073360w.
- [28] S.P. E, T.S. Miller, J.V. Macpherson, P.R. Unwin, Controlled functionalisation of single-walled carbon nanotube network electrodes for the enhanced voltammetric detection of dopamine, *Phys. Chem. Chem. Phys.*, 17 (2015) 26394-26402. <https://doi.org/10.1039/C5CP04905A>.
- [29] I. Dumitrescu, J.P. Edgeworth, P.R. Unwin, J.V. Macpherson, Ultrathin carbon nanotube mat electrodes for enhanced amperometric detection, *Adv. Mater.*, 21 (2009) 3105-3109. <https://doi.org/10.1002/adma.200900402>.
- [30] F.A. Larik, A. Saeed, T.A. Fattah, U. Muqadar, P.A. Channar, Recent advances in the synthesis, biological activities and various applications of ferrocene derivatives, *Appl. Organomet. Chem.*, 31 (2017) e3664. <https://doi.org/10.1002/aoc.3664>.
- [31] C.J. Yu, H. Yowanto, Y.J. Wan, T.J. Meade, Y. Chong, M. Strong, L.H. Donilon, J.F. Kayyem, M. Gozin, G.F. Blackburn, uridine-conjugated ferrocene DNA oligonucleotides: Unexpected cyclization reaction of the uridine base, *J. Am. Chem. Soc.*, 122 (2000) 6767-6768. <https://doi.org/10.1021/ja994241m>.
- [32] E.S. Krider, T.J. Meade, Electron transfer in DNA: covalent attachment of spectroscopically unique donor and acceptor complexes, *J. Biol. Inorg. Chem.*, 3 (1998) 222-225. <https://doi.org/10.1007/s007750050225>.
- [33] R.E. Holmlin, J.A. Yao, J.K. Barton, Dipyridophenazine complexes of Os(II) as red-emitting DNA probes: Synthesis, characterization, and photophysical properties, *Inorg. Chem.*, 38 (1999) 174-189. <https://doi.org/10.1021/ic9808955>.

- [34] S.C. Hillier, S.E. Flower, C.G. Frost, A.T.A. Jenkins, R. Keay, H. Braven, J. Clarkson, An electrochemical gene detection assay utilising T7 exonuclease activity on complementary probe–target oligonucleotide sequences, *Electrochem. Commun.*, 6 (2004) 1227-1232. <https://doi.org/10.1016/j.elecom.2004.09.019>.
- [35] S.C. Hillier, C.G. Frost, A.T.A. Jenkins, H.T. Braven, R.W. Keay, S.E. Flower, J.M. Clarkson, An electrochemical study of enzymatic oligonucleotide digestion, *Bioelectrochemistry*, 63 (2004) 307-310. <https://doi.org/10.1016/j.bioelechem.2003.10.028>.
- [36] A.A. D'souza, R. Shegokar, Polyethylene glycol (PEG): a versatile polymer for pharmaceutical applications, *Expert Opin. Drug Deliv.*, 13 (2016) 1257-1275. DOI: 10.1080/17425247.2016.1182485.
- [37] I.M. Kuznetsova, K.K. Turoverov, V.N. Uversky, What macromolecular crowding can do to a protein, *Int. J. Mol. Sci.*, 15 (2014) 23090-23140. DOI: 10.3390/ijms151223090.
- [38] X. Zhang, P.J.J. Huang, M.R. Servos, J.W. Liu, Effects of polyethylene glycol on DNA adsorption and hybridization on gold nanoparticles and graphene oxide, *Langmuir*, 28 (2012) 14330-14337. <https://doi.org/10.1021/la302799s>
- [39] B. Akabayov, S.R. Akabayov, S.J. Lee, G. Wagner, C.C. Richardson, Impact of macromolecular crowding on DNA replication, *Nat. Commun.*, 4 (2013). DOI: 10.1038/ncomms2620.
- [40] T.-C. Cheng, K.-H. Chuang, M. Chen, H.-E. Wang, S.-C. Tzou, Y.-C. Su, C.-H. Chuang, C.-H. Kao, B.-M. Chen, L.-S. Chang, S.R. Roffler, T.-L. Cheng, Sensitivity of PEGylated interferon detection by anti-polyethylene glycol (PEG) antibodies depends on PEG length, *Bioconjugate Chem.*, 24 (2013) 1408-1413. DOI: 10.1021/bc3006144.

- [41] C. Ota, K. Takano, Behavior of bovine serum albumin molecules in molecular crowding environments investigated by Raman spectroscopy, *Langmuir*, 32 (2016) 7372-7382. <https://doi.org/10.1021/acs.langmuir.6b01228>.
- [42] N.R. Wilson, M. Guille, I. Dumitrescu, V.R. Fernandez, N.C. Rudd, C.G. Williams, P.R. Unwin, J.V. Macpherson, Assessment of the electrochemical behavior of two-dimensional networks of single-walled carbon nanotubes, *Anal. Chem.*, 78 (2006) 7006-7015. <https://doi.org/10.1021/ac0610661>.
- [43] A.G. Güell, A.S. Cuharuc, Y.R. Kim, G.H. Zhang, S.Y. Tan, N. Ebejer, P.R. Unwin, Redox-dependent spatially resolved electrochemistry at graphene and graphite step edges, *ACS Nano*, 9 (2015) 3558-3571. <https://doi.org/10.1021/acsnano.5b00550>.
- [44] P.V. Dudin, P.R. Unwin, J.V. Macpherson, Electro-oxidation of hydrazine at gold nanoparticle functionalised single walled carbon nanotube network ultramicroelectrodes, *Phys. Chem. Chem. Phys.*, 13 (2011) 17146-17152. <https://doi.org/10.1039/C1CP21937E>.
- [45] R. Saito, G. Dresselhaus, M.S. Dresselhaus, *Physical Properties of Carbon Nanotubes*, Imperial College Press, London, 1998.
- [46] A.F. Holloway, K. Toghill, G.G. Wildgoose, R.G. Compton, M.A.H. Ward, G. Tobias, S.A. Llewellyn, B. Ballesteros, M.L.H. Green, A. Crossley, Electrochemical opening of single-walled carbon nanotubes filled with metal halides and with closed ends, *J. Phys. Chem. C*, 112 (2008) 10389-10397. <https://doi.org/10.1021/jp802127p>.
- [47] M.S. Dresselhaus, G. Dresselhaus, R. Saito, A. Jorio, Raman spectroscopy of carbon nanotubes, *Phys. Rep.*, 409 (2005) 47-99. <https://doi.org/10.1016/j.physrep.2004.10.006>.

- [48] M.S. Dresselhaus, G. Dresselhaus, A. Jorio, A.G. Souza, R. Saito, Raman spectroscopy on isolated single wall carbon nanotubes, *Carbon*, 40 (2002) 2043-2061. [https://doi.org/10.1016/S0008-6223\(02\)00066-0](https://doi.org/10.1016/S0008-6223(02)00066-0).
- [49] V. Skakalova, A.B. Kaiser, W.U. Dettlaff, K. Hrnčarikova, S. Roth, Effect of chemical treatment on electrical conductivity, infrared absorption, and Raman spectra of single-walled carbon nanotubes, *J. Phys. Chem. B*, 109 (2005) 7174-7181. <https://doi.org/10.1021/jp044741o>.
- [50] A. Jorio, R. Saito, G. Dresselhaus, M.S. Dresselhaus, Determination of nanotubes properties by Raman spectroscopy, *Philos. T. Roy. Soc. A*, 362 (2004) 2311-2336. DOI: 10.1098/rsta.2004.1443.
- [51] S.C. Wang, K.S. Chang, C.J. Yuan, Enhancement of electrochemical properties of screen-printed carbon electrodes by oxygen plasma treatment, *Electrochim. Acta*, 54 (2009) 4937-4943. <https://doi.org/10.1016/j.electacta.2009.04.006>.
- [52] A. Jorio, A.G. Souza, G. Dresselhaus, M.S. Dresselhaus, R. Saito, J.H. Hafner, C.M. Lieber, F.M. Matinaga, M.S.S. Dantas, M.A. Pimenta, Joint density of electronic states for one isolated single-wall carbon nanotube studied by resonant Raman scattering, *Phys. Rev. B*, 63 (2001) 245416 (1-4). <https://doi.org/10.1103/PhysRevB.63.245416>
- [53] G. Zhang, A.S. Cuharuc, A.G. Güell, P.R. Unwin, Electrochemistry at highly oriented pyrolytic graphite (HOPG): lower limit for the kinetics of outer-sphere redox processes and general implications for electron transfer models, *Phys. Chem. Chem. Phys.*, 17 (2015) 11827-11838. <https://doi.org/10.1039/C5CP00383K>.

- [54] I. Dumitrescu, P.V. Dudin, J.P. Edgeworth, J.V. Macpherson, P.R. Unwin, Electron transfer kinetics at single-walled carbon nanotube electrodes using scanning electrochemical microscopy, *J. Phys. Chem. C*, 114 (2010) 2633-2639. <https://doi.org/10.1021/jp908830d>.
- [55] W.F. Sokol, D.H. Evans, Suppression of background current in differential pulse voltammetry with solid electrodes, *Anal. Chem.*, 53 (1981) 578-580. <https://doi.org/10.1021/ac00227a004>.
- [56] S.J. Cobb, J.V. Macpherson, Enhancing square wave voltammetry measurements via electrochemical analysis of the non-faradaic potential window, *Anal. Chem.*, 91 (2019) 7935-7942. <https://doi.org/10.1021/acs.analchem.9b01857>
- [56] P.R. Unwin, A.G. Güell, G. Zhang, Nanoscale electrochemistry of sp² carbon materials: from graphite and graphene to carbon nanotubes, *Acc. Chem. Res.*, 49 (2016) 2041-2048. <https://doi.org/10.1021/acs.accounts.6b00301>.
- [57] I. Dumitrescu, P.R. Unwin, J.V. Macpherson, Electrochemical impedance spectroscopy at single-walled carbon nanotube network ultramicroelectrodes, *Electrochem. Commun.*, 11 (2009) 2081-2084. <https://doi.org/10.1016/j.elecom.2009.08.057>.
- [57] A.G. Güell, K.E. Meadows, P.V. Dudin, N. Ebejer, J.V. Macpherson, P.R. Unwin, Mapping nanoscale electrochemistry of individual single-walled carbon nanotubes, *Nano Lett.*, 14 (2014) 220-224. <https://doi.org/10.1021/nl403752e>.
- [58] C.E. Hotchen, I.J. Maybury, G.W. Nelson, J.S. Foord, P. Holdway, F. Marken, Amplified electron transfer at poly-ethylene-glycol (PEG) grafted electrodes, *Phys. Chem. Chem. Phys.*, 17 (2015) 11260-11268. <https://doi.org/10.1039/C5CP01244A>.

[59] A.J. Downard, A.D. Roddick, Effect of electrochemical pretreatment on protein adsorption at glassy-carbon electrodes, *Electroanalysis*, 6 (1994) 409-414. <https://doi.org/10.1002/elan.1140060509>.

[60] E. Celik, L. Liu, H. Choi, Protein fouling behavior of carbon nanotube/polyethersulfone composite membranes during water filtration, *Water Res.*, 45 (2011) 5287-5294. <https://doi.org/10.1016/j.watres.2011.07.036>.